STK11 prevents melanoma invasion through STAT3/5 and FAK repression

Journal:	*Journal of Investigative Dermatology*
Manuscript ID	JID-2020-1006
Article Type:	Original Article
Date Submitted by the Author:	20-Nov-2020
Complete List of Authors:	Dzung, Andreas; University Hospital Zurich, Department of Dermatology Saltari, Annalisa; University Hospital Zurich, Department of Dermatology Tiso, Natascia; University of Padova, Department of Biology Lyck, Ruth; University of Bern, Theodor Kocher Institute Dummer, Reinhard; University of Zurich Medical School, Department of Dermatology Levesque, Mitchell; University Hospital Zurich, Department of Dermatology
Keywords:	Melanoma, Metastasis, Drug Resistance, Cancer Biology, Signaling

STK11 prevents melanoma invasion through STAT3/5 and FAK repression.

Andreas Dzung[1*], Annalisa Saltari[1*], Natascia Tiso[2], Ruth Lyck[3],

Reinhard Dummer[1] & Mitchell P. Levesque[1]

[1]Department of Dermatology, University of Zurich Hospital, Zurich, Switzerland,

[2]Laboratory of Developmental Genetics, Department of Biology, University of Padova, Italy

[3]Theodor Kocher Institute, University of Bern, Bern, Switzerland

*these authors equally contributed to this work

Corresponding author:

Mitchell P. Levesque, University of Zurich Hospital, University of Zurich, Wagistrasse 14, CH 8952 Schlieren, Switzerland

Tel: +41 44 556 32 62;

e-mail: mitchell.levesque@usz.ch

Running title: Role of STK11 in melanoma

Keywords: Melanoma, metastasis, Drug resistance, cancer biology, signaling

ABSTRACT

The serine/threonine kinase 11 (STK11/LKB1) is a tumor suppressor involved in metabolism and cell motility. In $BRAF^{V600E}$ melanoma, STK11 is inactivated by ERK and Rsk, leading to its inability to bind and activate AMPK and promoting melanoma cell proliferation[20]. Although STK11 mutations occur in 5-10% of cutaneous melanoma, few functional studies have been performed. By knocking out STK11 using the CRISPR/Cas9 technology in two human BRAF-mutant melanoma cell lines, we found that STK11-loss favors BRAFi-resistance and leads to a more invasive phenotype both *in vitro* and *in vivo* in a zebrafish xenograft model. Furthermore, while STK11 was expressed in primary human melanoma tumors, the expression significantly decreased in melanoma metastases and was lowest in brain metastases. In the STK11-knockout cells we observed increased activating phosphorylation of STAT3/5 and FAK. Using inhibitors of STAT3/5 and FAK, we were able to revert the invasive phenotype. Our findings confirm an increased invasive phenotype upon STK11-inactivation in BRAF-mutant melanoma that can be targeted by STAT3/5 and FAK-inhibition.

INTRODUCTION

The LKB1/*STK11* gene encodes a Serine/Threonine kinase, which is broadly expressed in all fetal and adult tissues although at different levels.[1,2] STK11 is known to directly phosphorylate and regulate adenosine monophosphate-activated protein kinase (AMPK) and 12 other AMPK-like kinases to regulate a broad spectrum of cellular functions including growth, metabolism, autophagy, adhesion, and polarity.[3,4] It was first reported to be a tumor suppressor when genetic loss of function alterations of STK11 were identified as the major cause of Peutz-Jeghers syndrome (PJS). PJS is a rare, autosomal dominant disease with hemizygotic loss of STK11 in 95-100% of the cases.[5–8] It is characterized by the growth of gastrointestinal hamartomous polyps, hyperpigmented freckling of the mouth, lips, fingers or toes, and a strong predisposition for cancer in different organs, such as colon, pancreas, breast, ovary and testis.[7,9,10] Moreover, STK11 mutations are frequently found in a variety of cancer patients without PJS, such as lung adenocarcinoma (30%), cervical carcinoma (15%) and melanoma (5-10%)[11–15]. Due to its high mutation rate in lung cancer it has been frequently studied and was shown to increase lung cancer aggressiveness, metastasis, immune-evasion and recently anti-PD1-inhibitor resistance.[16–19]

In cutaneous melanoma, oncogenic $BRAF^{V600E}$, but not BRAF wildtype signaling has been shown to functionally inhibit some STK11-dependent pathways[20]: Through direct binding and through increased ERK-activity, STK11 was not able to activate AMPK, a key metabolic enzyme, showing a linkage between the hyperactivated Mitogen Activated Protein Kinase (MAPK) pathway with the STK11-AMPK pathway. These findings imply an important role of the suppression of STK11 activity in $BRAF^{V600E}$ -driven melanoma tumorigenesis.[20,21] Furthermore, the genetic inactivation of STK11 in a genetically engineered KRAS-mutant melanoma mouse model led to highly metastatic melanoma with 100% penetrance in a SRC family kinase-dependent manner. As BRAF-

mutant melanoma represent around 50% of cutaneous melanomas[22], we sought to study the effects of genetic STK11-inactivation in $BRAF^{V600E}$ -mutant human melanoma cells on BRAF-inhibitor resistance and invasion.

RESULTS

STK11-Loss Contributes to Resistance Against BRAF^{V600E}-Inhibition.

To explore the role of STK11-inactivation in melanoma we created stable STK11-knockouts (STK11 KO) using the Clustered Regularly Interspaced Short Palindromic Repeats (CRISPR) and CRISPR-associated protein-9 nuclease CRISPR/Cas9 system[23]. To knock out STK11, we used three different short-guide RNAs (sgRNA), each targeting a different exon in the STK11-transcript (Figure 1A). To rule out differences based on cell line heterogeneity, we generated monoclonal cell lines from the BRAF^{V600E}-mutated melanoma cell cultures M990922 and WM793B. For each cell line we expanded single cell clones with a successful knock-out on at least two different exons and one single cell clone harboring a non-targeting scramble (SCR) short-guide RNA construct with wildtype STK11 (Figure S 1A and 1B). We then evaluated whether, in the absence of treatment, STK11 loss was associated with increased cell growth and we observed no difference in the proliferation rate between the transgenic STK11 KO cells and the SCR cells (Figure 1 C). In fact, although STK KO2 in both cell lines showed a significant increase in cell growth at 3 days in comparison to controls, the same effect was not observed in STK11 KO1 and KO3 (Figure S 1B and S 1C).

We then investigated if STK11 loss-of-function influenced resistance to BRAF-inhibition. In a 2-dimensional (2D) assay, the viability under the BRAF-inhibitor (BRAFi) LGX818 (LGX) was decreased in comparison to DMSO in both STK SCR and KO cells (Figure 1D). However, STK loss, resulted in a significantly decreased susceptibility to LGX treatment compared to the control at both 3 and 6 days, suggesting a role for STK11 in drug resistance. A similar result was shown in a long-term 14d colony formation assay (Figure S 1D).

To confirm the same findings in a model which better reflects the in vivo situation, we generated 3-dimensional (3D) multi-cellular spheroids after seeding the cells on agarose coated plates (Figure S 1E).

Consistently with the previous results, when we treated 3D spheroids with LGX and performed a live (green) / dead (red) staining, a significantly higher amount of dead cells were stained in the SCR constructs compared to the STK11 KO cells (Figure 1E)

Activation of AMPK-RAPTOR Pathway Upon BRAFi is Prevented in STK11 Knockout Cells

A possible mechanism for increased resistance to BRAFi in STK11-KO cells could be the loss of the previously well-described tumor suppressor function through AMPK, in which STK11-induced activation of AMPK inhibits the mTOR pathway.[3,4,24,25] As previously reported, hyperactive MAPK-signaling in $BRAF^{V600E}$-mutant melanoma suppresses the interaction between STK11 and AMPK through strong phospho-ERK1/2 signaling.[20] We therefore expect that in STK11 expressing $BRAF^{V600E}$ mutant melanoma, the tumor suppressive STK11-AMPK axis is not active, but is rather inhibited through $BRAF^{V600E}$ signaling (Figure 2A, left). We hypothesized that, under BRAF-inhibition, STK11 could restore its tumor suppressive function and induce Raptor signaling through AMPK activation (Figure 2A, middle). Finally, in STK11 KO cells, we expect that the activation of AMPK-Raptor pathway upon BRAF-inhibition is prevented and associated with increased resistance (Figure 2A, right).

To test this hypothesis, we treated the transgenic M990922 and WM793 constructs with LGX over 72h. LGX-treatment effectively reduced the phosphorylation of the $BRAF^{V600E}$ downstream kinase ERK1/2.

Interestingly, in SCR clones, STK11-levels increased upon LGX treatment confirming the role of $BRAF^{V600E}$ in inhibiting STK11 activity (Figure 2B). As expected, AMPKα1 threonine 172-phosphorylation levels increased under LGX treatment as compared to their untreated baseline levels, indicating increased AMPKα1 activation (Figure 2B). In contrast, AMPKα1 activation was prevented in STK11 KO cells. Consistently, phosphorylation of the AMPKα1-target Raptor serine 172, increased in the SCR cells under treatment but not in STK11 KO cells (Figure 2B).

To evaluate whether the inhibition of the AMPKα1-Raptor axis in STK11 KO clones could be reverted, we treated WM793B and M990922 STK11 KO cells with AICAR, an analog of adenosine monophosphate (AMP) capable of stimulating AMPK activity (Figure 2C). Interestingly, AMPK phosphorylation was restored in the presence of AICAR and resulted in a significant decrease of melanoma viability in STK11 KO clones (Figure 2C and 2D). Moreover, the administration of AICAR increased the effectiveness of the BRAFi by significantly reducing the cell viability in comparison to the single treatment (Figure 2E).

STK11 Loss Induces Invasion of $BRAF^{V600E}$ Melanoma Cells *in vitro*

As the loss of STK11 has been recently shown to increase invasion in a genetically modified mouse KRAS-mutant melanoma model[15], we assessed the effect of STK11-loss on invasion in BRAF-mutated melanoma. First, we tested the ability of the STK11 constructs to adhere to dermal microvascular (HMEC1) and blood-brain barrier (HDMEC/D3) endothelial cells. The adhesion of STK11 KO cells to the monolayer of endothelial cells was significantly higher compared to control cells, suggesting a greater ability to invade the tumor microenvironment (Figure 3A).

To measure the invasive abilities of STK11-KO cells in a more complex model, we embedded 3D-multicellular spheroids of the transgenic cell lines into collagen I. Over 7 days and 16 days, the

STK11-KO cells displayed a significantly increased invasion, as compared to the SCR cells, into the collagen I matrix (Figure 3B). Notably, treatment of the collagen-embedded spheres with LGX, led to a strong reduction of collagen invasion in all the transgenic constructs. However, while invasion was completely prevented by LGX in the SCR cell lines, the STK11-KO cells showed residual invasive capabilities under BRAF-inhibition displaying a significantly higher invasion area compared to the control cells even in the presence of LGX as well as increased viability (Figure S 2A, S 2B and S 2C).

STK11 Loss Is Associated with Increased Metastasis in Zebrafish Xenografts and in Melanoma Patients

To evaluate the effects of STK11-KO in $BRAF^{V600E}$ melanoma *in vivo*, we employed zebrafish xenografts. We injected M990922 and WM793B STK11 constructs into the yolk of 2-day old zebrafish larvae, exposed them to LGX 1 day post-injection (dpi) and assessed the fish for survival and metastasis formation 6 days post-injection (dpi). At 1dpi, melanoma cells were confined into the yolk of zebrafish larvae (Figure S 3A). However, at 6 dpi, STK11 KO cells strongly migrated from the yolk to other tissues showing a significantly higher number of zebrafish with metastasis in comparison to scramble cells (Figure 4A and 4B). No difference in survival was observed between the xenografts, except for a higher mortality of M990922 STK11 KO injected zebrafish (Figure S 3B). Consistent with the *in vitro* results, despite a strong reduction of invasion upon LGX treatment in both cell lines, STK11-KO injected larvae displayed a significantly higher percentage of metastasis also in the presence of the treatment (Figure 4A, 4B and Figure S 2C). Interestingly, the analysis of the sites of metastasis revealed an increased occurrence of brain metastases in WM793B STK11 KO cells (Figure S 3D).

As loss of function mutations of STK11 are less common in melanoma (10%) [12–14] we wondered whether the expression of STK11 changes during the course of melanoma progression. We thus evaluated STK11 and S100 expression, a marker for melanoma cells[26] in three tissue micro arrays (TMAs) derived from 1) primary melanoma tumors (n=166), 2) melanoma metastases from different non-cranial organ sites (n=82), and 3) melanoma brain metastases (N=70) (Figure 4C). In primary melanoma tumors, STK11 was heterogeneously expressed. Moreover, STK11 levels were significantly lower in melanoma metastases in comparison to primary melanomas, with the lowest expression in brain metastases (Figure 4C and 4D).

STK11 Loss Enhanced Activation of STAT3/5 and FAK

To identify possible pathways that might be involved in STK11-inactivation induced invasion and metastasis, we performed a phospho-kinase protein array in M990922 cells (Figure 5A). When we compared the phosphorylation pattern of STK11 constructs, we observed a significantly higher activation of STAT3, STAT5a/b and FAK in STK11 KO in comparison to control cells (Figure 5B). Consistently, the phosphorylation of these proteins was stronger in both WM793 and M990922 STK11 KO cell lines (Figure 5C). Moreover, upon LGX administration pERK was significantly reduced in both cell lines, while AMPK phosphorylation was detected only in control but not in STK11 KO cells confirming the role of STK11 in AMPK activation. Finally, pSTAT5a/b was significantly higher in STK11 KO cells irrespective of the presence of the BRAFi (Figure 5D).

STK11 Loss-Mediated Invasion Is Prevented by STAT3/5- and FAK-inhibition

We next tested the effect of STAT3/5 (C188-9 and SH-4-54) and FAK (PF-573228) inhibitors on viability and invasion of 3D melanoma spheroids under increasing drug concentrations (Figure S

3A). Interestingly, the inhibition of STAT3/5 or FAK strongly reduced the invasive abilities of M990922 and WM793B STK11 KO cells without affecting melanoma viability (Figure S 3A). Quantification of the spheroid area revealed a significantly reduced invasion of STK11 KO spheres after treatment with pSTAT3/5i or pFAKi in both M990922 and WM793B cell lines (Figure 6 A, 6B and 6C). A similar result was observed after administration of both drugs in combination, with an induction of cell death in the presence of the highest concentrations (Figure S 4B and S4C). We therefore conclude that STAT3/5 and FAK pathway are inhibited in STK11 expressing cells. On the contrary, STK11 loss, is associated with increased invasive phenotype in vitro and in vivo, which can be reverted by the inhibition of STAT3/5 and FAK activation (Figure 6D).

DISCUSSION

The role of the tumor suppressor STK11 has been frequently studied in many cancers, often in the context of invasion and metastasis[1,3,17], and loss of STK11 has recently also been associated with immune evasion and decreased response in immune-checkpoint inhibitor therapy in lung cancer.[18,19] However, its role in melanoma remains to be extensively investigated. This study highlights the role of STK11 in melanoma drug resistance and invasion. In detail, the evaluation of drug response revealed an increase resistance of STK11 KO cells towards BRAF inhibition both *in vitro* and *in vivo*. Moreover, we showed that the higher sensitivity of STK11 SCR cells to the BRAFi LGX, was associated with the activation of STK11-AMPK-RAPTOR pathway. Consistently, AMPK signaling inhibited mTOR, which has been previously linked with melanoma survival and resistance.[27,28]

We observed that the most dramatic phenotypic change resulting from STK11-KO was increased invasiveness. Compared to the SCR cells, the STK11-KO cells displayed an enhanced adhesion to to endothelial cells, suggesting an increased ability to migrate, and a strong invasion of collagen I in a 3D-multicellular spheroid model. Consistently, STK11-KO cells were more invasive in a *in vivo* zebrafish xenograft model, showing a significant higher percentage of metastasis in comparison to SCR injected larvae. These observations strengthen previous findings in KRAS-mutant melanoma mouse models[15] and suggest that STK11-inactivation increases invasion also in a BRAF V^{600E} mutant background.

While STK11 loss of function mutations are less frequent in melanoma than in other cancers (10% and less)[12,14,29], non-genetic mechanisms of STK11 inactivation can take place, such as epigenetic inactivation, decreased expression or biological inactivation.[30] The evaluation of STK11 level on melanoma tissue microarrays (TMAs) revealed that STK11 was highly expressed in primary

tumors but significantly decreased in melanoma metastases with the lowest levels observed in brain melanoma metastasis. This finding is consistent with previous observations in non-small-cell lung carcinoma where an oncogenic KRAS mutation and low STK11 copy number was shown to be associated with brain metastasis[31]. Additionally, STK11 deletion is frequently shown in brain metastases of different carcinomas[32].

To investigate the mechanisms driving the enhanced invasion in STK11-KO cells compared to the SCR cells, we performed a phospho-kinase array screen. In the STK11-KO cells we identified an increased activating phosphorylation of STAT3 (serine 727 and tyrosine 705), STAT5A/B (tyrosine 694/699) and FAK (tyrosine 397).

Increased activity of p-STAT3 upon STK11 loss or downregulation has been shown in many cancers: in papillary thyroid carcinoma cells STK11 has been shown to inhibit STAT3-activation via RET/PTC inhibition.[33] In addition, STK11 was shown to directly interact with STAT3, by leading to the suppression of STAT3-mediated gene expression. On the contrary, STK11-knockdown results in increased transactivation of STAT3 and cell proliferation.[33] In gastrointestinal cancer, loss of STK11 in stromal fibroblast cells was associated with the induction of the IL-11/JAK/STAT3 pathway, which resulted in fully penetrant polyposis in mice and inflammation.[34] Interestingly, in a mouse model of PJS, the heterozygous deletion of STK11 in T cells was sufficient to promote gastrointestinal polyp formation, STAT3 activation and increased expression of IL-6, IL-11 and CXCL2.[35] Moreover, STAT3 has been consistently associated with cell migration, invasion and metastasis in many cancers including melanoma, where STAT3 activation promoted melanoma brain metastasis in a xenograft mouse model.[36–38] While the regulation of STAT5A/B through STK11 has not been extensively studied, it has been frequently associated with metastasis in different cancers. In prostate cancer cells p-STAT5 Y694/699

promoted metastatic behavior and JAK2-STAT5A/B signaling was critical for the induction of epithelial-mesenchymal transition[39,40]. In colorectal cancer cells, STAT5 silencing induced G1 cell cycle arrest and reduced tumor cell invasion[41]. In melanoma, more malignant and metastatic phenotypes were governed by the scavenger receptor SR-BI which in turn activated STAT5 through glycosylation.[42]

Finally, the focal adhesion kinase FAK/PTK2 is another well described target of STK11, which have been extensively studied in adhesion, invasion and metastatic processes. In lung cancer cells, STK11 forms a complex with FAK to repress its activation , thereby inhibiting the adhesion to fibronectin.[43] Likewise, in a lung cancer mouse model with KRAS hyperactivation and STK11 loss, a strong FAK activation occurred in collectively invasive cells: when these cells were tested in a 3D invasion model the loss of STK11, but not P53, was sufficient to drive invasion, which was highly sensitive to FAK inhibition.[44] In aggressive uveal and cutaneous melanoma cells, FAK was phosphorylated on its key tyrosine residues Y397 and Y576 and correlated with an increased invasion, migration and vasculogenic mimicry plasticity.[45]

Interestingly, the inhibition of STAT3/5 and FAK in STK11 KO melanoma cells had no effects on the viability of 3D spheroids. On the contrary, the administration of STAT3/5 and FAK -inhibitors successfully reverted their invasive phenotype. In conclusion, STK11-loss is associated with increased resistance to BRAFi through the inhibition of AMPK-RAPTOR axis. The administration of the AMPK inducer AICAR, reverts the phenotype by increasing the sensitivity to the BRAFi. In addition, STK11 KO leads to STAT3/5 and FAK-mediated invasion. These results highlight the prognostic role of STK11 in melanoma metastasis and show a potential for the use of AICAR in combination with STAT3/5 or FAK-inhibitors for the treatment of $BRAF^{V600E}$ mutated melanoma.

MATERIAL AND METHODS

Cell Culture

Human primary melanoma cells were obtained from the URPP melanoma biobank Zurich (mitchelpaul.levesque@usz.ch) or from the American Type Culture Collection (ATCC, https://www.lgcstandards-atcc.org/) and cultured as indicated in Supplementary Material.

Transgenic cell lines

To create transgenic knock-out cell lines of STK11, the Clustered Regularly Interspaced Short Palindromic Repeats (CRISPR) and CRISPR-associated protein-9 nuclease (CRISPR/Cas9) system was used as indicated in Supplementary Material. For transduction of melanoma cells, the virus-containing medium was added together with PEImax and polybrene (8µg/mL). GFP-positive cells were sorted as single cells by the FACSAria™ III fluorescence-activated cell sorter (BD Biosciences).

Colorimetric Resazurin-based viability assay:

Cells were seeded into 96-well plates and treated 1d post-seeding with LGX818 (Selleckchem, Cat.no. S7108), AICAR (Selleckchem, Cat.No. S1802) and viability was assessed as indicated in Supplementary Material.

Colony formation assay:

100 or 500 cells/well were seeded in 12-well plates and treated with LGX. Medium was changed every 72h. The staining and the quantification of the number of colonies was perfomed as indicated in Supplementary Material.

3D-multicellular spheroid assay and spheroid collagen invasion assay:

3D-melanoma spheroids were obtained by seeding melanoma cells on previously coated agarose plate. The spheroids were treated for drug response assessment or embedded into a collagen I-mixture as indicated in Supplementary Material. The spheres viability was assessed by calcein AM (live) (Sigma, Cat.No. 17783) and ethidium homodimer (death) stain (Sigma, Cat.No. 46043) as indicated in Supplementary Material.

Endothelial-melanoma cell-cell adhesion assay:

The imicrovascular endothelial cells hMEC1 and hCMEC/D3 were seeded into a 4-well chamber slide (Falcon, Cat.No. 354114) (25'000 cells per 1.7cm^2 chamber) and grown to 100% confluency (ca 4d). Melanoma cells were stained with Vybrant DiI (1 µg/mL, ThermoFisher, Cat.No. V22885) and incubated at 37°C with endothelial monolayers. The evaluation of adherent cells was performed as indicated in Supplementary Material.

Western Blots:

Protein extracts were obtained by using the cell lysis buffer (NaCl 150mM, MgCl2 15mM, EGTA 1mM, Hepes 50mM, Glycerol 10%, Triton-X 1%) and Western Blot was performed as indicated in Supplementary Material. The following antibodies were used: STK11 (CST #3047), ERK1/2 (CST #4695), p-ERK1/2 T202/Y204 (CST# 4376), STAT3 (CST #9132), p-STAT3 Y705 (#9138), p-STAT3 S727 (CST #9134), FAK (CST #3285), p-FAK Y397 (CST #3283), p-STAT5A/B Y699/Y694 (CST #9359S).

Immunohistochemistry:

The TMAs of primary melanomas were a gift from the URPP biobank Zurich, University Hospital Zurich, Switzerland (Mitch Levesque), while the TMA from non-cranial melanoma metastases was purchased from Biomax (Cat.No. BCC38218). The TMA from brain metastasis was described before[51]. Immunohistochemistry was performed on tissue microarrays (TMAs) by using as indicated in Supplementary Material.

Human Phospho-Kinase Array Kit

The Proteome Profiler Human Phospho-Kinase Array Kit (R&D systems, Cat. No. ARY003B) was performed as indicated by the manufacturer. The quantification of phosphorylated protein was performed as indicated in Supplementary Material.

Zebrafish husbandry

Zebrafish xenograft experiments were performed in collaboration with Professor Natascia Tiso at the zebrafish facility of the University of Padova, Italy. Larvae were injected at 2 days after fertilization with melanoma cells as indicated in the Supplementary Materials.

Statistical analysis

All statistical analysis were performed using GraphPad Prism 5.0. P values ≤ 0.05 were considered significant. All experiments with cell lines were performed in triplicates and error bars represent the mean ± S.D.

CONFLICT OF INTEREST

The authors state no conflicts of interest.

ACKNOWLEDGMENTS

We thank Florian Olomski for his aid in cloning. We thank Federica Sella (University Hospital Zurich) for the immunohistochemical stains. We further thank Patrick Turko and Phil Cheng for biostatistical analyses and Melanie Maudrich, Jan Kaesler and Corinne Stoffel for various help in experiments in the laboratory (University Hospital Zurich).

REFERENCES

1. Zhao, R.-X. & Xu, Z.-X. Targeting the LKB1 Tumor Suppressor. *Curr. Drug Targets* **15**, 32–52 (2014).

2. Tissue expression of STK11 - Summary - The Human Protein Atlas. https://www.proteinatlas.org/ENSG00000118046-STK11/tissue.

3. Momcilovic, M. & Shackelford, D. B. Targeting LKB1 in cancer – exposing and exploiting vulnerabilities. *Br. J. Cancer* **113**, 574–584 (2015).

4. Shackelford, D. B. & Shaw, R. J. The LKB1–AMPK pathway: metabolism and growth control in tumour suppression. *Nat. Rev. Cancer* **9**, 563–575 (2009).

5. Hemminki, A. *et al.* A serine/threonine kinase gene defective in Peutz–Jeghers syndrome. *Nature* **391**, 184–187 (1998).

6. Aretz, S. *et al.* High proportion of large genomic STK11 deletions in Peutz-Jeghers syndrome. *Hum. Mutat.* **26**, 513–519 (2005).

7. Daniell, J., Plazzer, J.-P., Perera, A. & Macrae, F. An exploration of genotype-phenotype link between Peutz-Jeghers syndrome and STK11: a review. *Fam. Cancer* **17**, 421–427 (2018).

8. Nagy, R., Sweet, K. & Eng, C. Highly penetrant hereditary cancer syndromes. *Oncogene* **23**, 6445–6470 (2004).

9. Resta, N. *et al.* Cancer risk associated with STK11/LKB1 germline mutations in Peutz–Jeghers syndrome patients: Results of an Italian multicenter study. *Dig. Liver Dis.* **45**, 606–611 (2013).

10. Peutz-Jeghers Syndrome. *Cancer.Net* https://www.cancer.net/cancer-types/peutz-jeghers-syndrome (2012).

11. Abildgaard, C. & Guldberg, P. Molecular drivers of cellular metabolic reprogramming in melanoma. *Trends Mol. Med.* **21**, 164–171 (2015).

12. Forbes, S. A. *et al.* COSMIC: mining complete cancer genomes in the Catalogue of Somatic Mutations in Cancer. *Nucleic Acids Res.* **39**, D945-950 (2011).

13. Guldberg, P. *et al.* Somatic mutation of the Peutz-Jeghers syndrome gene, LKB1/STK11, in malignant melanoma. *Oncogene* **18**, 1777–1780 (1999).

14. Rowan, A. *et al.* Somatic mutations in the Peutz-Jeghers (LKB1/STKII) gene in sporadic malignant melanomas. *J. Invest. Dermatol.* **112**, 509–511 (1999).

15. Liu, W. *et al.* LKB1/STK11 Inactivation Leads to Expansion of a Prometastatic Tumor Subpopulation in Melanoma. *Cancer Cell* **21**, 751–764 (2012).

16. Ji, H. *et al.* LKB1 modulates lung cancer differentiation and metastasis. *Nature* **448**, 807–810 (2007).

17. Marcus, A. I. & Zhou, W. LKB1 regulated pathways in lung cancer invasion and metastasis. *J. Thorac. Oncol. Off. Publ. Int. Assoc. Study Lung Cancer* **5**, 1883–1886 (2010).

18. Koyama, S. *et al.* STK11/LKB1 Deficiency Promotes Neutrophil Recruitment and Proinflammatory Cytokine Production to Suppress T-cell Activity in the Lung Tumor Microenvironment. *Cancer Res.* **76**, 999–1008 (2016).

19. Skoulidis, F. *et al.* STK11/LKB1 Mutations and PD-1 Inhibitor Resistance in KRAS-Mutant Lung Adenocarcinoma. *Cancer Discov.* **8**, 822–835 (2018).

20. Zheng, B. *et al.* Oncogenic B-RAF Negatively Regulates the Tumor Suppressor LKB1 to Promote Melanoma Cell Proliferation. *Mol. Cell* **33**, 237–247 (2009).

21. Li, N., Huang, D., Lu, N. & Luo, L. Role of the LKB1/AMPK pathway in tumor invasion and metastasis of cancer cells (Review). *Oncol. Rep.* **34**, 2821–2826 (2015).

22. Schadendorf, D. *et al.* Melanoma. *The Lancet* **392**, 971–984 (2018).

23. Jinek, M. *et al.* A programmable dual-RNA-guided DNA endonuclease in adaptive bacterial immunity. *Science* **337**, 816–821 (2012).

24. Sebbagh, M., Olschwang, S., Santoni, M.-J. & Borg, J.-P. The LKB1 complex-AMPK pathway: the tree that hides the forest. *Fam. Cancer* **10**, 415–424 (2011).

25. Zhou, W., Marcus, A. I. & Vertino, P. M. Dysregulation of mTOR activity through LKB1 inactivation. *Chin. J. Cancer* **32**, 427–433 (2013).

26. Jungbluth, A. A. & Busam, K. J. 29 - Immunohistochemistry for the Diagnosis of Melanocytic Proliferations. in *Pathology of Melanocytic Tumors* (eds. Busam, K. J., Gerami, P. & Scolyer, R. A.) 348–363 (Elsevier, 2019). doi:10.1016/B978-0-323-37457-6.00029-8.

27. Kozar, I., Margue, C., Rothengatter, S., Haan, C. & Kreis, S. Many ways to resistance: How melanoma cells evade targeted therapies. *Biochim. Biophys. Acta BBA - Rev. Cancer* **1871**, 313–322 (2019).

28. Rossi, A. *et al.* Drug resistance of BRAF-mutant melanoma: Review of up-to-date mechanisms of action and promising targeted agents. *Eur. J. Pharmacol.* **862**, 172621 (2019).

29. STK11 - My Cancer Genome. https://www.mycancergenome.org/content/gene/stk11/#ref-3.

30. Zhou, W., Zhang, J. & Marcus, A. I. LKB1 tumor suppressor: Therapeutic opportunities knock when LKB1 is inactivated. *Genes Dis.* **1**, 64–74 (2014).

31. Zhao, N. *et al.* Alterations of LKB1 and KRAS and Risk of Brain Metastasis: Comprehensive Characterization by Mutation Analysis, Copy Number, and Gene Expression in Non-Small-Cell Lung Carcinoma. *Lung Cancer Amst. Neth.* **86**, 255–261 (2014).

32. Sobottka, S. B. *et al.* Frequent Loss of Heterozygosity at the 19p13.3 Locus Without LKB1/STK11 Mutations in Human Carcinoma Metastases to the Brain. *J. Neurooncol.* **49**, 187–195 (2000).

33. Kim, D. W. *et al.* Tumor Suppressor LKB1 Inhibits Activation of Signal Transducer and Activator of Transcription 3 (STAT3) by Thyroid Oncogenic Tyrosine Kinase Rearranged in Transformation (RET)/Papillary Thyroid Carcinoma (PTC). *Mol. Endocrinol.* **21**, 3039–3049 (2007).

34. Ollila, S. *et al.* Stromal Lkb1 deficiency leads to gastrointestinal tumorigenesis involving the IL-11–JAK/STAT3 pathway. *J. Clin. Invest.* **128**, 402–414 (2018).

35. Poffenberger, M. C. *et al.* LKB1 deficiency in T cells promotes the development of gastrointestinal polyposis. *Science* **361**, 406–411 (2018).

36. Teng, Y., Ross, J. L. & Cowell, J. K. The involvement of JAK-STAT3 in cell motility, invasion, and metastasis. *JAK-STAT* **3**, (2014).

37. Kulesza, D. W., Przanowski, P. & Kaminska, B. Knockdown of STAT3 targets a subpopulation of invasive melanoma stem-like cells. *Cell Biol. Int.* **43**, 613–622 (2019).

38. Xie, T. *et al.* Activation of Stat3 in Human Melanoma Promotes Brain Metastasis. *Cancer Res.* **66**, 3188–3196 (2006).

39. Gu, L. *et al.* Stat5 promotes metastatic behavior of human prostate cancer cells in vitro and in vivo. *Endocr. Relat. Cancer* **17**, 481–493 (2010).

40. Talati, P. G. *et al.* Jak2-Stat5a/b Signaling Induces Epithelial-to-Mesenchymal Transition and Stem-Like Cell Properties in Prostate Cancer. *Am. J. Pathol.* **185**, 2505–2522 (2015).

41. Xiong, H. *et al.* Inhibition of STAT5 induces G1 cell cycle arrest and reduces tumor cell invasion in human colorectal cancer cells. *Lab. Invest.* **89**, 717–725 (2009).

42. Kinslechner, K. *et al.* Malignant Phenotypes in Metastatic Melanoma are Governed by SR-BI and its Association with Glycosylation and STAT5 Activation. *Mol. Cancer Res. MCR* **16**, 135–146 (2018).

43. Kline, E. R., Shupe, J., Gilbert-Ross, M., Zhou, W. & Marcus, A. I. LKB1 Represses Focal Adhesion Kinase (FAK) Signaling via a FAK-LKB1 Complex to Regulate FAK Site Maturation and Directional Persistence. *J. Biol. Chem.* **288**, 17663–17674 (2013).

44. Gilbert-Ross, M. *et al.* Targeting adhesion signaling in KRAS, LKB1 mutant lung adenocarcinoma. *JCI Insight* **2**,.

45. Hess, A. R. *et al.* Focal Adhesion Kinase Promotes the Aggressive Melanoma Phenotype. *Cancer Res.* **65**, 9851–9860 (2005).

46. Walter, D. M. *et al.* Systematic In Vivo Inactivation of Chromatin-Regulating Enzymes Identifies Setd2 as a Potent Tumor Suppressor in Lung Adenocarcinoma. *Cancer Res.* **77**, 1719–1729 (2017).

47. Shalem, O. *et al.* Genome-Scale CRISPR-Cas9 Knockout Screening in Human Cells. *Science* **343**, 84–87 (2014).

48. CHOPCHOP v3: expanding the CRISPR web toolbox beyond genome editing | Nucleic Acids Research | Oxford Academic. https://academic.oup.com/nar/article/47/W1/W171/5491735.

49. Guzmán, C., Bagga, M., Kaur, A., Westermarck, J. & Abankwa, D. ColonyArea: An ImageJ Plugin to Automatically Quantify Colony Formation in Clonogenic Assays. *PLOS ONE* **9**, e92444 (2014).

50. Westerfield, M. The zebrafish book. A guide for the laboratory use of zebrafish (Danio rerio). (University of Oregon Press, 2000).

51. García-Martín AB, Zwicky P, Gruber T, et al. VLA-4 mediated adhesion of melanoma cells on the blood–brain barrier is the critical cue for melanoma cell intercalation and barrier disruption. Journal of Cerebral Blood Flow & Metabolism. 2019;39(10):1995-2010. doi:10.1177/0271678X18775887

FIGURE LEGENDS

Figure 1. STK11 Loss Contributes to Resistance Against $BRAF^{V600E}$-Inhibition.

A) STK11 KO sgRNA (KO 1-3) targets on different exon on the STK11 transcript. B) Western Blot of SCR and STK11 KO clones. C) 2000 cells (M990922) and 3000 cells (WM793B) were seeded in 96-well plates and 2D MTT viability assay was performed overtime. D) STK11 SCR and STK11 KO clones were seeded in 96-well plates. 1 day later, cells were treated with LGX 10nM and viability was measured by Resazurin assay 3d and 6d later. E) 4000 cells per well were seeded in agar-coated plates until spheres formed and treated with LGX 50nM for 3d and 6d. Live/dead ratios were assessed by Calcein-AM/Ethidium-homodimer staining. Data represent the mean ± S.D. of triplicate determinations. Two-way Anova was used for statistical analysis *p<0.05; **p<0.01; ***p<0.001; ****p<0.00001

Figure 2. Activation of AMPK-RAPTOR Pathway Upon BRAFi is Prevented in STK11 Knockout Cells.

A) Model explaining the loss of the tumor suppressive function of the STK11-AMPKα axis in STK11 KO cells. B) WB of M990922 and WM793B under treatment with LGX 20nM. C) Western Blot of M990922 and WM793B with the AMPK-activator AICAR (1mM) alone or in combination with LGX (20nM). D and E) 2D viability assay under 6d of AICAR mono-treatment or in combination with LGX by Resazurin. Data represent the mean ± S.D. of triplicate determinations. Two-way Anova was used for statistical analysis *p<0.05; **p<0.01; ***p<0.001; ****p<0.00001

Figure 3. STK11 Loss Induces Invasion of BRAFV600E Melanoma Cells *in vitro*

A) Cellular adhesion assay. Human microvascular endothelial cells hMEC1 (skin-derived) and hCMEC/D3 (blood-brain barrier derived) were seeded and grown to 100% confluency. Melanoma cells were starved for 24h, fluorescently labeled and 25'000 cells were seeded per cell culture chamber. After an incubation of 30min at 37°C the chambers were washed and the number of adhered and fluorescently labeled cells was assessed. B) 3D multicellular spheroid invasion into collagen. After spheroid formation, the spheres were embedded into collagen and assessed for invasion at 7d and 16d. Data represent the mean ± S.D. of triplicate determinations. Two-way Anova was used for statistical analysis *p<0.05; **p<0.01; ***p<0.001; ****p<0.00001

Figure 4. STK11 Loss Is Associated with Increased Metastasis in Zebrafish Xenografts and in Melanoma Patients

A) Fluorescently labeled M990922 and WM793B cells were injected into the yolk of 2 days post-fertilization (dpf) old zebrafish as a single droplet (100 µm diameter, about 100 cells/embryo). B) The numbers of zebrafish with metastases was assessed at 6 dpf by a blind investigator. Data represents the mean ± S.D. of triplicate determinations. Two-way Anova was used for statistical analysis *p<0.05; **p<0.01; ***p<0.001; ****p<0.00001 C) Immunohistochemical stainings for S100 and STK11 were performed on two tissue micro arrays (TMA) of human primary melanoma tumors (N=166), of non-cranial (N=82) and on brain metastases (N=70). D) Quantification of melanoma STK11+ cells was performed by QuPath. The average of 10 areas was calculated and normalized to S100. One-way Anova was used for statistical analysis *p<0.05; **p<0.01; ***p<0.001; ****p<0.00001

Figure 5. STK11 Loss Enhanced Activation of STAT3/5 and FAK

A) A human phospho-kinase array was performed on M990922 SCR and STK11 KO at 24h both under vehicle (DMSO) and LGX 20nM treatment. B) Comparative analysis of the vehicle treated cells. One-way Anova was used for statistical analysis. *p<0.05; **p<0.01; ***p<0.001 C) Confirmation of differential STAT3/5- and FAK-phosphorylation by WB in both M990922 and WM793B. D) Comparative analysis of vehicle treated cells with LGX-treated cells. Two-way Anova was used for statistical analysis. *p<0.05; **p<0.01; ***p<0.001

Figure 6. STK11 Loss-Mediated Invasion Is Prevented by STAT3/5- and FAK-inhibition

A) Collagen-embedded spheroids were treated with STAT3/5 (SH-45-4 and C188-9) and FAK (PF-573228) -inhibitors at 5μM for M990922 and at 20μM (SH-45-a) and 10 μM (PF-573228) for WM793B. 3 spheres/condition were used to calculate the area of invasion. Two-way Anova was used for statistical analysis. *p<0.05; **p<0.01; ***p<0.001C) Pooled analysis of M990922 and WM793 confirmed the suppressive effects of STAT3/5- and FAK-inhibitors (STAT3/5i and FAKi) on invasion. D) Graphical conclusion. STK11 knockout leads to a STAT3/5 and FAK-dependent increase of invasion that can be targeted, using STAT3/5i and FAKi.

Figure S1 Evaluation of STK11 constructs viability

A) Transgenic cell line generation. For both cell cultures, M990922 and WM793B, a monoclonal cell line was created. These cell lines were transduced with SCR (non-targeting sgRNA), STK11 KO1, STK11 KO2 and STK11 KO3 sgRNA/Cas9 constructs. For each cell line, one SCR and two KO-clones were amplified. B) and C) MTT assay of STK11 SCR vs STK11 KO. Data represent the mean ± S.D. of triplicate determinations. Two-way Anova was used for statistical analysis

*p<0.05; **p<0.01; ***p<0.001; ****p<0.00001 D) Colony formation assay. 3500 cells per well were seeded into a 24w plate and treated with LGX 10nM. E) 3D multicellular cells successfully formed 4d after seeding 4000 cells per well into an agarose coated 96 well plate.

Figure S2 Evaluation of sensitivity to BRAFi in SCR vs STK11 KO melanoma cells in 2D and 3D models

A) Collagen-embedded spheroids were treated with LGX 50nM for 7d and 16d. B) 3 spheres/condition were used to calculate the area of invasion. Two-way Anova was used for statistical analysis. *p<0.05; **p<0.01; ***p<0.001 C) 3D spheres were treated with LGX for 16d and viability was evaluated by Calcein-AM/Ethidium homodimer staining. Live/dead ratio was quantified with Photoshop. 6 spheres/condition were quantified. Two-way Anova was used for statistical analysis. *p<0.05; **p<0.01; ***p<0.001

Figure S3 Evaluation of metastasis formation in SCR vs STK11 KO injected zebrafish larvae

A) The yolk of 2d old Zebrafish larvae was injected with human melanoma cell lines and assessed on the next day (1dpi) for successful injection, before treatment start. B) The survival of the embryos under vehicle and LGX treatment, was assessed until 6d. C) and D) At 6d post-transplantation under vehicle and LGX treatment, the injected fish were assessed for fluorescently-labeled metastases outside the yolk for both, M990922 and WM793B by a blind investigator. D) Evaluation of brain metastasis in SCR and STK11 KO injected zebrafish

Figure S4 The treatment with pSTAT3/5i and/or pFAKi reverts the invasive phenotype of STK11 KO spheres.

A) and B) M990922 and WM793B were treated with increasing concentrations of STAT3/5 (SH-45-4 and C188-9) and FAK (PF-573228) –inhibitors alone or in combination. After 16d the viability of spheres was assessed by Calcein-AM/Ethidium homodimer staining. C) Live/dead ratio was quantified with Photoshop. 6 spheres/condition were quantified. Two-way Anova was used for statistical analysis. *$p<0.05$; **$p<0.01$; ***$p<0.001$

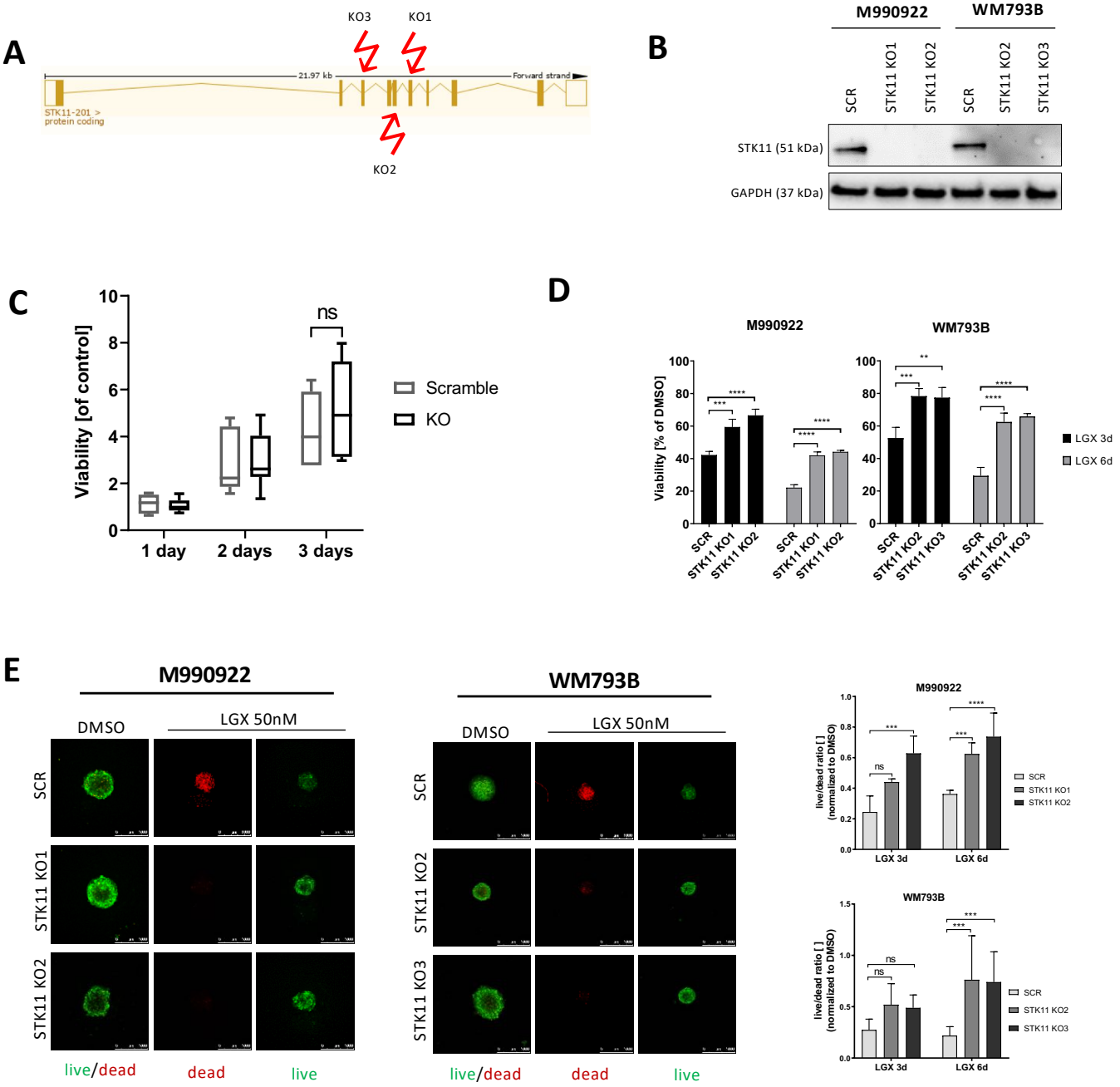

Figure 1. STK11 Loss Contributes to Resistance Against BRAF^{V600E}-Inhibition

A) STK11 KO sgRNA (KO 1-3) targets on different exon on the STK11 transcript. B) Western Blot of SCR and STK11 KO clones. C) 2000 cells (M990922) and 3000 cells (WM793B) were seeded in 96-well plates and 2D MTT viability assay was performed overtime. D) STK11 SCR and STK11 KO clones were seeded in 96-well plates. 1 days later, cells were treated with LGX 10nM and viability was measured by Resazurin assay 3d and 6d later. E) 4000 cells per well were seeded in agar-coated plates until spheres formed and treated with LGX 50nM for 3d and 6d. Live/dead ratios were assessed by Calcein-AM/Ethidium-homodimer staining. Data represent the mean ± S.D. of triplicate determinations. Two-way Anova was used for statistical analysis *p<0.05; **p<0.01; ***p<0.001; ****p<0.00001

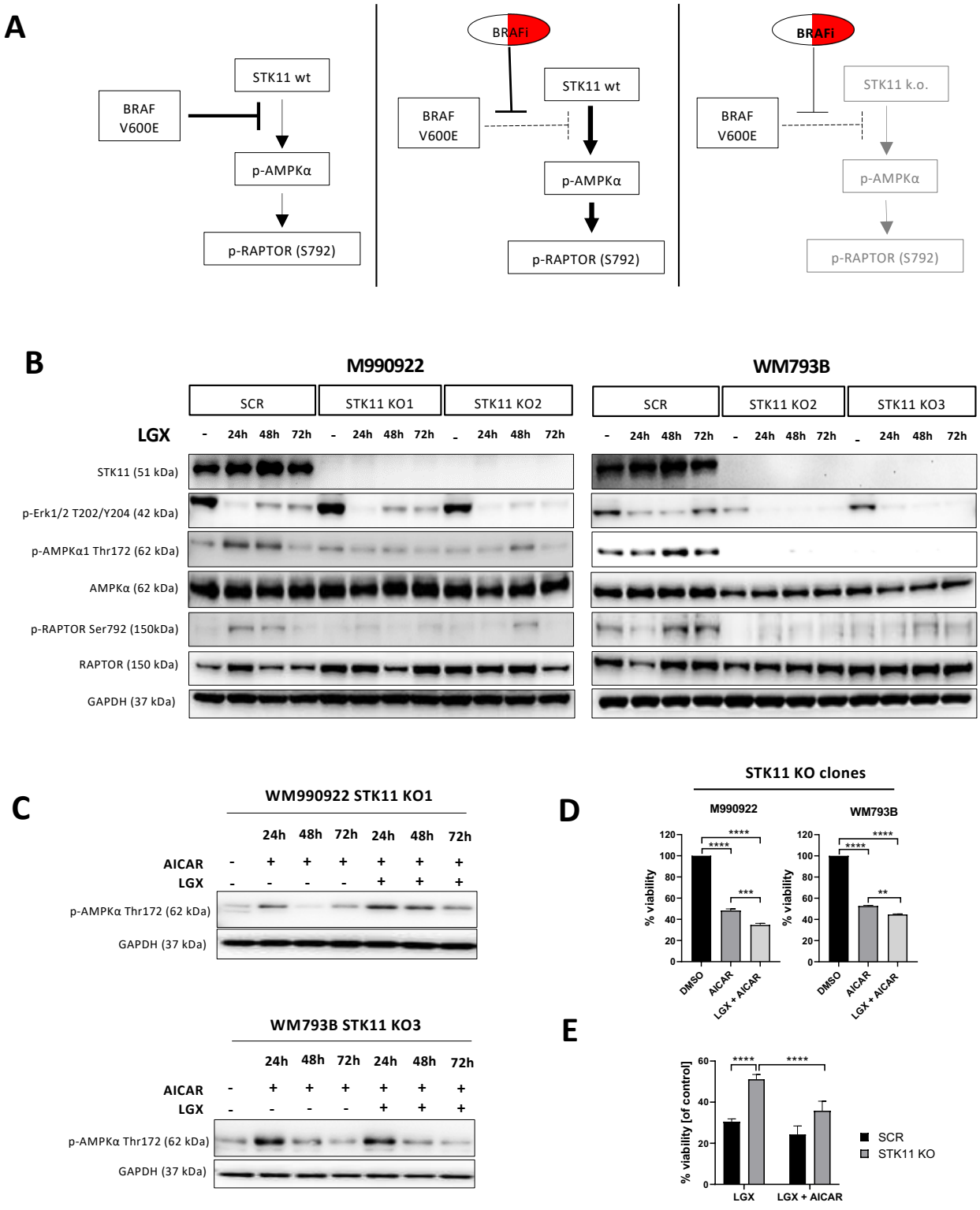

Figure 2. Activation of AMPK-RAPTOR Pathway Upon BRAFi is Prevented in STK11 Knockout Cells. A) Model explaining the loss of the tumor suppressive function of the STK11-AMPKα axis in STK11 KO cells. B) WB of M990922 and WM793B under treatment with LGX 20nM. C) Western Blot of M990922 and WM793B with the AMPK-activator AICAR (1mM) alone or in combination with LGX (20nM). D) and E) 2D viability assay under 6d of AICAR mono-treatment or in combination with LGX by Resazurin. Data represent the mean ± S.D. of triplicate determinations. Two-way Anova was used for statistical analysis *p<0.05; **p<0.01; ***p<0.001; ****p<0.00001

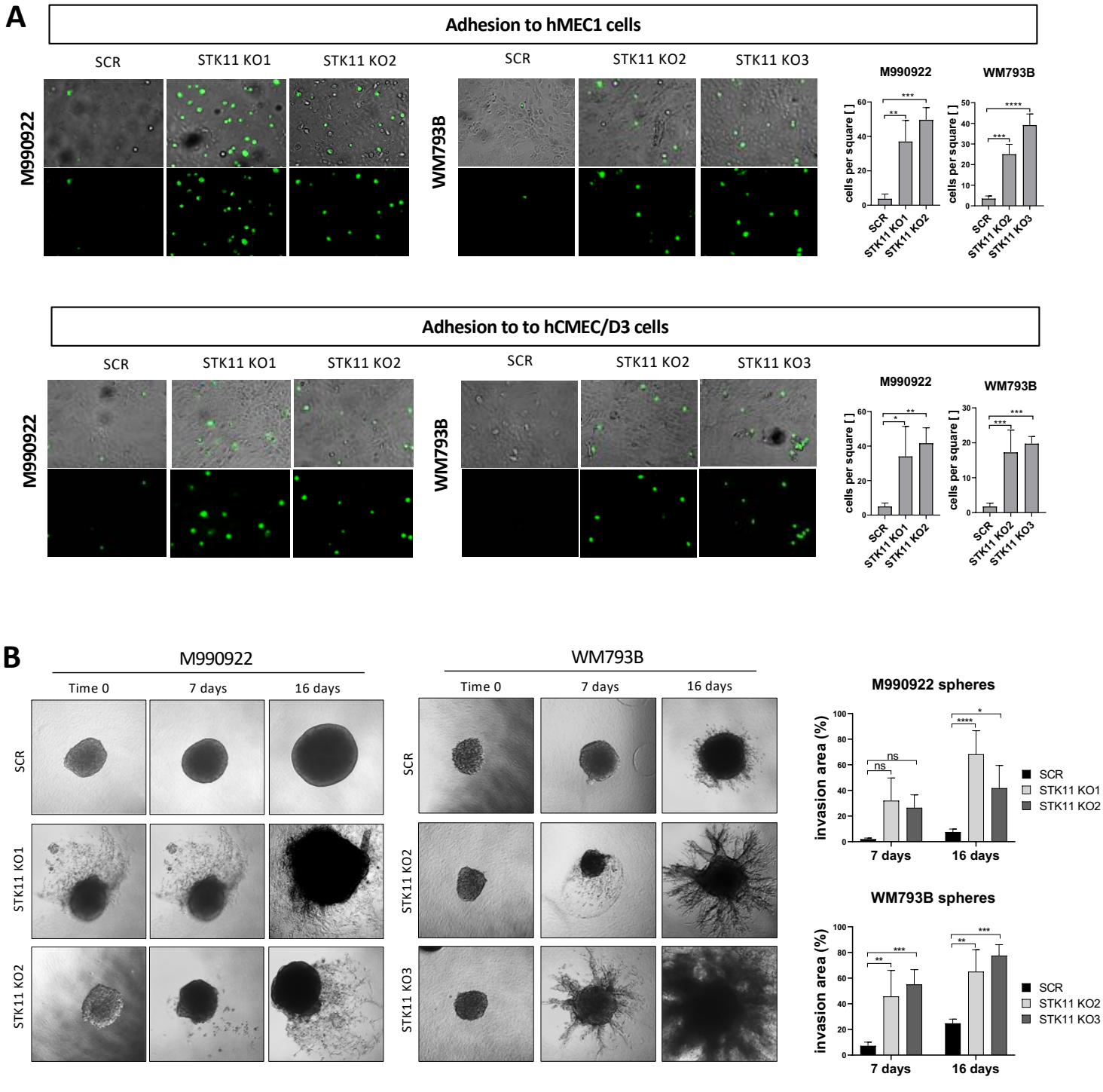

Figure 3. STK11 Loss Induces Invasion of BRAFV600E Melanoma Cells in vitro

A) Cellular adhesion assay. Human microvascular endothelial cells hMEC1 (skin-derived) and hCMEC/D3 (blood-brain barrier derived) were seeded and grown to 100% confluency. Melanoma cells were starved for 24h, fluorescently labeled and 25'000 cells were seeded per cell culture chamber. After an incubation of 30min at 37°C the chambers were washed and the number of adhered and fluorescently labeled cells was assessed. B) 3D multicellular spheroid invasion into collagen. After spheroid formation, the spheres were embedded into collagen and assessed for invasion at 7d and 16d. Data represent the mean ± S.D. of triplicate determinations. Two-way Anova was used for statistical analysis *p<0.05; **p<0.01; ***p<0.001; ****p<0.00001

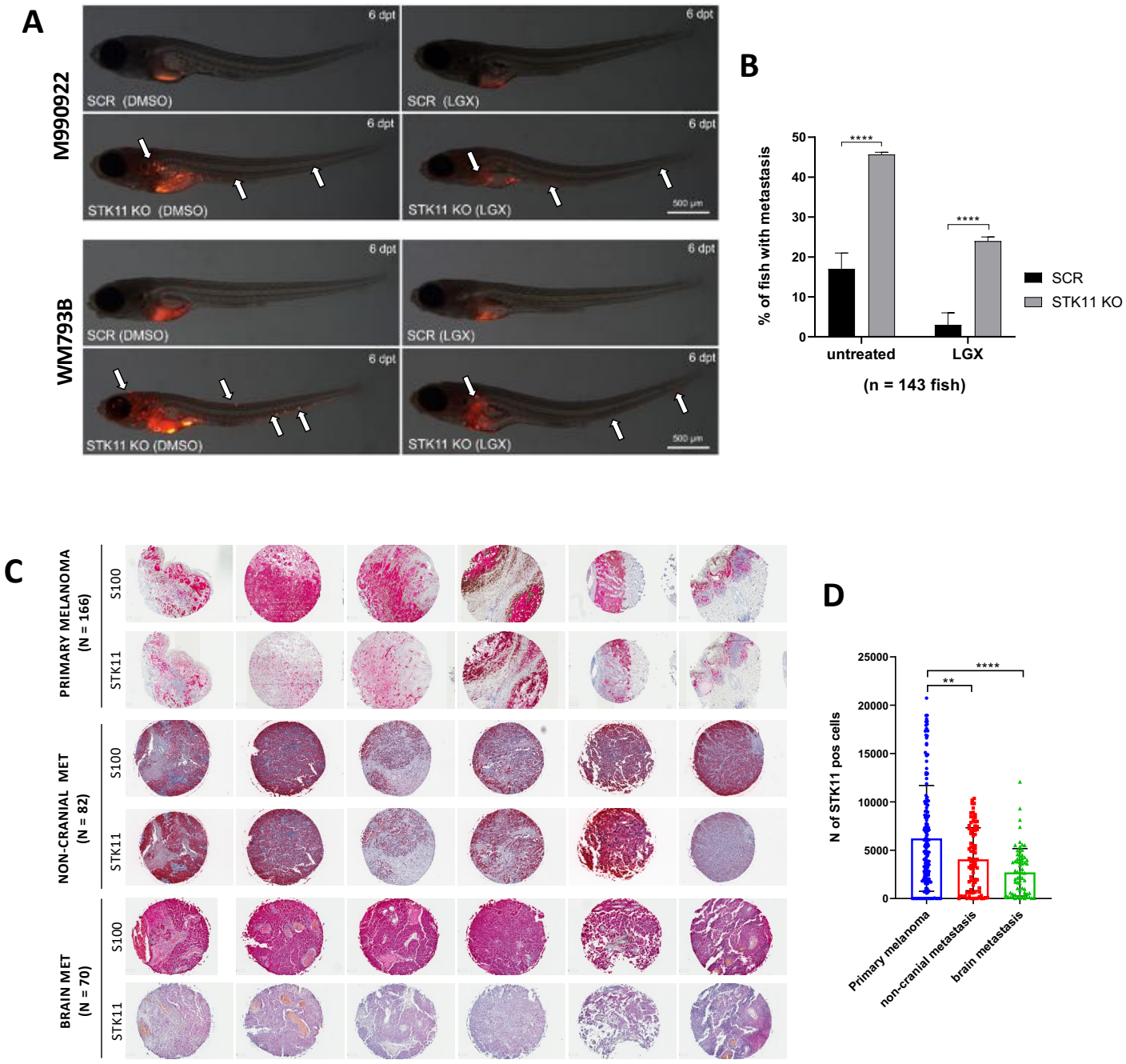

Figure 4. STK11 Loss Is Associated with Increased Metastasis in Zebrafish Xenografts and in Melanoma Patients

A) Fluorescently labeled M990922 and WM793B cells were injected into the yolk of 2 days post-fertilization (dpf) old zebrafish as a single droplet (100 µm diameter, about 100 cells/embryo). B) The numbers of zebrafish with metastases was assessed at 6 dpf by a blind investigator. Data represents the mean ± S.D. of 2 independent experiments. Two-way Anova was used for statistical analysis. *p<0.05; **p<0.01; ***p<0.001 C) Immunohistochemical stainings for S100 and STK11 were performed on two tissue micro arrays (TMA) of human primary melanoma tumors (N=166), of non-cranial (N=82) and on with brain metastases (N=70). D) Quantification of melanoma STK11+ cells was performed by QuPath. The average of 10 areas was calculated and normalized to S100. One-way Anova was used for statistical analysis *p<0.05; **p<0.01; ***p<0.001; ****p<0.00001

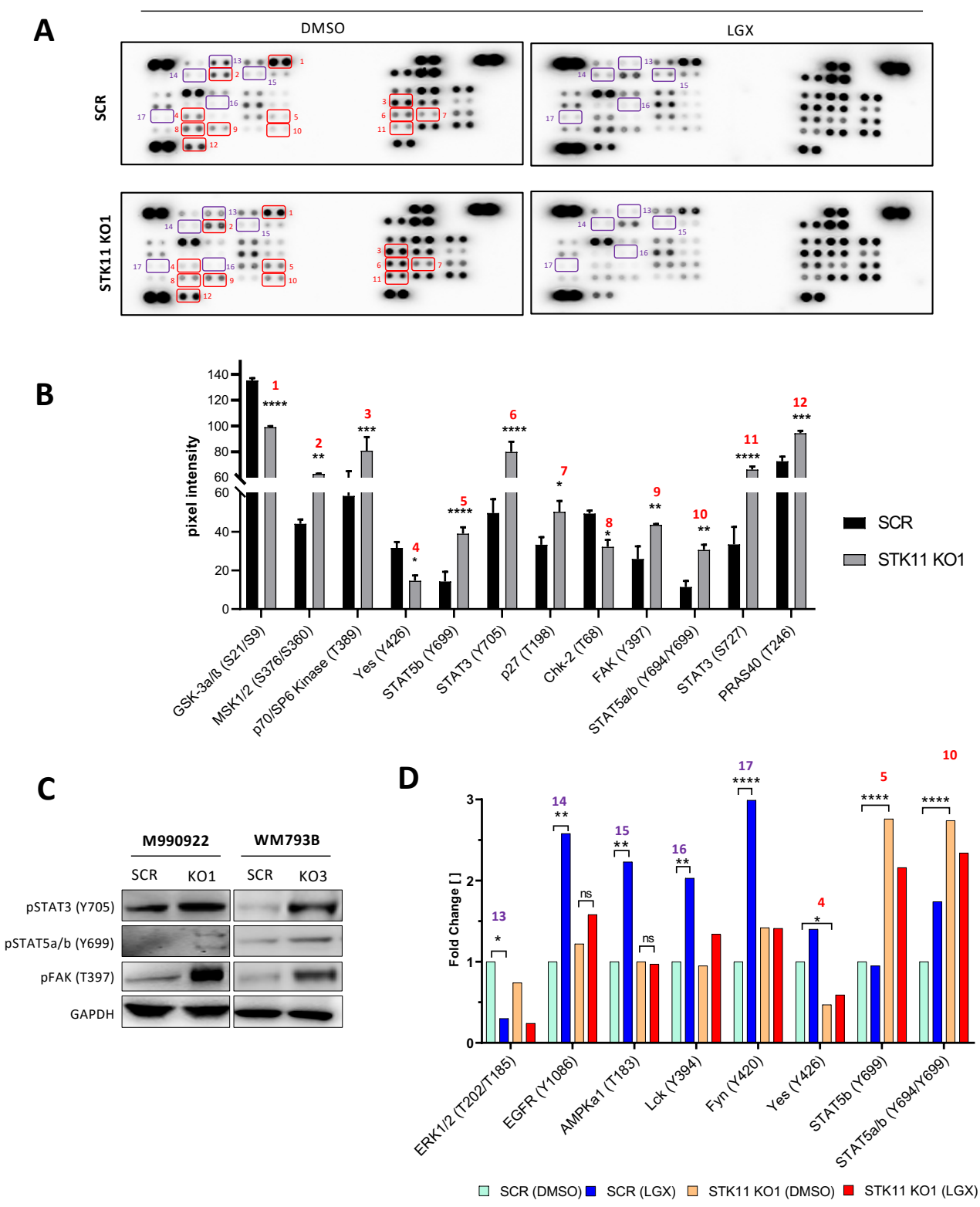

Figure 5. STK11 Loss Enhanced Activation of STAT3/5 and FAK

A) A human phospho-kinase array was performed on M990922 SCR and STK11 KO at 24h both under vehicle (DMSO) and LGX 20nM treatment. B) Comparative analysis of the vehicle treated cells. One-way Anova was used for statistical analysis. *p<0.05; **p<0.01; ***p<0.001 C) Confirmation of differential STAT3/5- and FAK-phosphorylation by WB in both M990922 and WM793B. D) Comparative analysis of vehicle treated cells with LGX-treated cells. Two-way Anova was used for statistical analysis. *p<0.05; **p<0.01; ***p<0.001

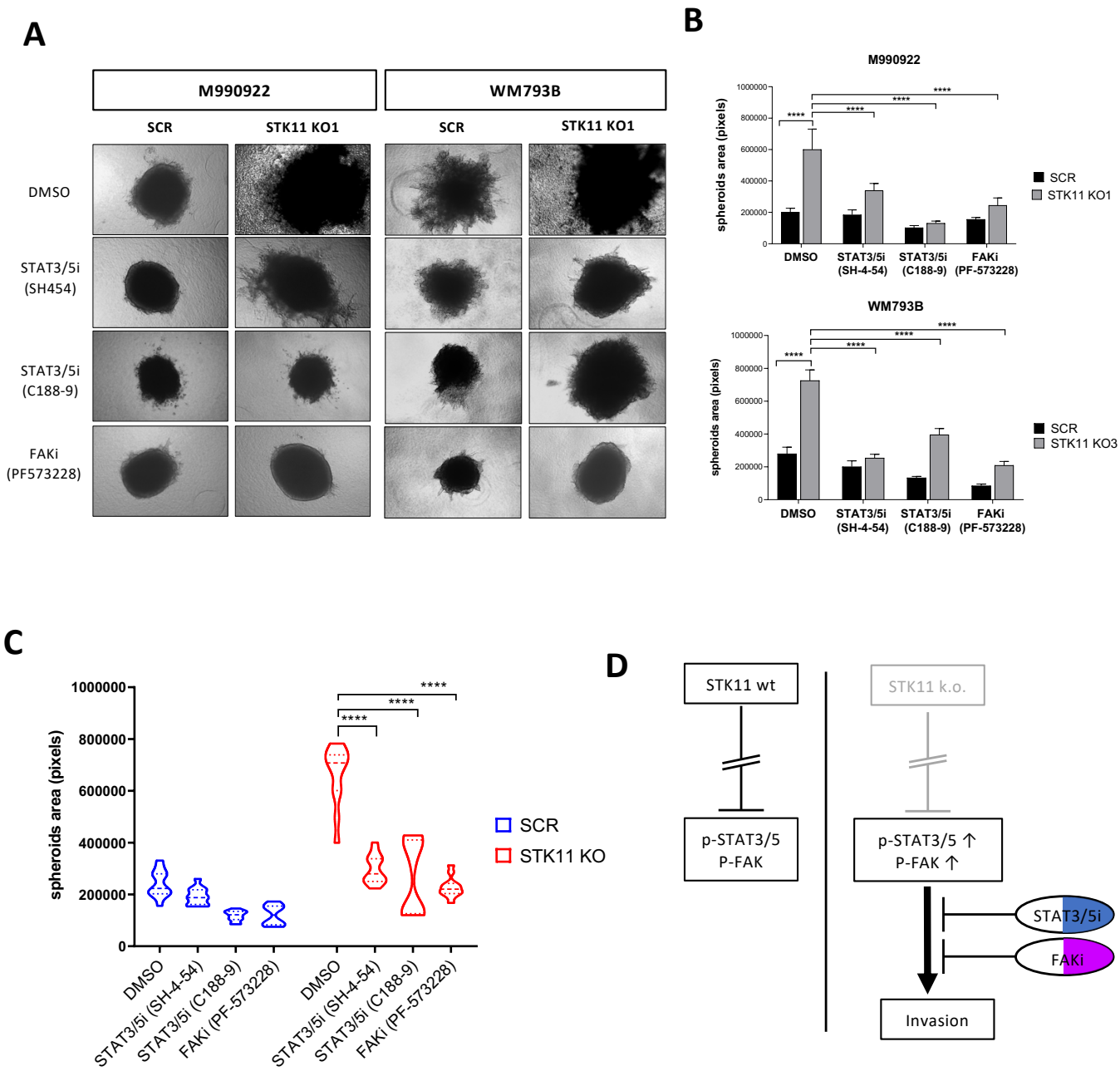

Figure 6. STK11 Loss-Mediated Invasion Is Prevented by STAT3/5- and FAK-inhibition

A) Collagen-embedded spheroids were treated with STAT3/5 (SH-45-4 and C188-9) and FAK (PF-573228) -inhibitors at 5μM for M990922 and at 20μM (SH-45-a) and 10 μM (PF-573228) for WM793B. B) 3 spheres/condition were used to calculate the area of invasion. Two-way Anova was used for statistical analysis. *p<0.05; **p<0.01; ***p<0.001 C) Pooled analysis of M990922 and WM793 confirmed the suppressive effects of STAT3/5- and FAK-inhibitors (STAT3/5i and FAKi) on invasion. D) Graphical conclusion. STK11 knockout leads to a STAT3/5 and FAK-dependent increase of invasion that can be targeted, using STAT3/5i and FAKi.

SUPPLEMENTARY MATERIAL

Material and methods

Human primary melanoma cells were obtained from the URPP melanoma biobank Zurich (mitchelpaul.levesque@usz.ch) or from the American Type Culture Collection (ATCC, https://www.lgcstandards-atcc.org/). M990922 (URPP biobank) and WM793B (ATCC) carried activating BRAFV600E-mutations and M130425 carried activating NRASQ61?-mutations. Human melanoma cells were cultured in RPMI 1640 medium (Sigma, Cat.No. R0883-500ML) supplemented with heat-inactivated FBS (10%, Pan Biotech, Cat.No. P30-1902, Lot.No. P160605), L-Glutamine (2mM, Gibco, Cat.No. 25030-024), Sodium-Pyruvate (1 mM, Sigma, Cat.No. S8636) and Normocin-Antimicrobial reagent (1x, InvivoGen, Cat.No. ant-nr-1) in a cell culture incubator (37°C, 5% CO2, 95% relative Humidity). The HEK293T cells (ATCC, Cat. No. CRL-3216) were cultured in DMEM with L-Glutamine and Pyruvate (Gibco, Cat.No. 41966-029) supplemented with heat-inactivated FBS (10%, Pan Biotech, Cat.No. P30-1902, Lot.No. P160605) and Pen-Strep (1%, Sigma, Cat.No. P4333-100ML) The immortalized microvascular endothelial cell lines hMEC1 (ATCC, Cat.No. CRL-3243) and hCMEC/D3 (Millipore, Cat.No. SCC066) were cultured in EndoGro MV complete medium adapted for human microvascular endothelial cells (Millipore, Cat.No. SCME004) and substituted with fibroblast growth-factor basic protein (bFGF) (1ng/mL, Millipore, Cat.No. GF003). Passaging: Cells were detached by removing the cell culture medium, washing with PBS ph7.4 (Gibco, Cat.No. 100010-015) followed by incubation with 0.05% Trypsin-EDTA (Gibco, Cat.No. 25300-054) in the recommended amount for the used cell culture dish (37°C, 1-3min). The trypsin was blocked with the appropriate serum-containing cell culture medium.

Transgenic cell lines

Expression plasmid creation:

Knockout: To create transgenic knock-out cell lines of STK11, the Clustered Regularly Interspaced Short Palindromic Repeats (CRISPR) and CRISPR-associated protein-9 nuclease (CRISPR/Cas9) system was used. We used the LentiCRISPRv2GFP (provided by David Feldser[46], Addgene plasmid #82416) and followed the Zhang lab protocol[47] for the single guide RNA (sgRNA) insertion into the LentiCRISPRv2GFP-plasmid. We used the following sequences for our sgRNAs that have been identified using the sgRNA design tool CHOPCHOP (https://chopchop.cbu.uib.no)[48]:

STK11 sgRNA1 (KO1) targeting STK11 exon 6 (GGGTCTGTACCCCTTCGAAG), STK11 sgRNA2 (KO2) targeting STK11 exon 5 (AGGCCGTTGGCAATCTCGGG), STK11 sgRNA3 (KO3) targeting STK11 exon 3 (GCTCATCGGCAAGTACCTGA), and a non-targeting scrambled sequence (SCR) sgRNA (GAACAGTCGCGTTTGCGACT). The process of the virus production and cell transduction will be described separately below.

Lentivirus production and cell transduction:

To produce the lentivirus necessary for the creation of the transgenic cell lines, 3.5*10^6 HEK293T cells were seeded into a 10cm dish for transfection with the viral plasmids. After 24h, each of the altered LentiCRISPRv2GFP expression plasmid now containing STK11 sgRNA 1, 2 or 3 or SCR sgRNA (4µg) was mixed with the packaging plasmid psPAX2 (2µg, provided by Didier Trono, Addgene plasmid #12260) and the envelope plasmid pMD2.G (1µg, provided by Didier Trono, Addgene plasmid #12259) and PEImax (21µg, Polysciences, Cat.No. 24765) in 1 mL of serum-free DMEM (Gibco, Cat.No. 11960-044) and incubated for 15 minutes at RT. The DNA/PEImax mixture was then added dropwise to the HEK293T cells. 24h post-transfection the medium was exchanged with 20mL HEK293T cell culture medium.

This virus-containing medium was collected after 48h and sterile filtered using a 0.2 µm sterile filter to remove any residual HEK293T cells. For transduction, 100µL of the virus-containing medium were added together with polybrene (8µg/mL) to the requested cells that were 80% confluent in a 6-well. GFP-positive cells were sorted as single cells into a 96-well plate by the FACSAria™ III fluorescence-activated cell sorter (BD Biosciences), raised and assessed for successful knock-out.

Cellular Assays

Colorimetric Resazurin-based viability assay:

Cells were seeded into 96-well plates and treated 1d post-seeding for 72h and/or 144h with LGX818 (Selleckchem, Cat.no. S7108), AICAR (Selleckchem, Cat.No. S1802) or the combination thereof in the stated concentrations. Triplicates were seeded for each condition. For the IC50-evaluation against LGX818, different wells were treated with ascending concentrations of the drug. At the day of assessment, the medium was exchanged with cell-culture medium containing Resazurin sodium salt (0.015mg/mL, Sigma-Aldrich, Cat.No. R7017) and incubated for 1.5h (37°C). The amount of metabolized fluorescent resorufin, which correlates with the amount of living cells was read at 535nm excitation and 595 emission.

Colony formation assay:

Cells were seeded in 12-well plates and treated with LGX for the indicated duration. Medium was changed every 72h. To assess the colonies the cells were fixed and stained with a filtered crystal violet solution (Crystal violet 0.05%w/v, Formaldehyde 1%, Methanol 1%, in PBS) for 20min at room temperature and washed with water. The plates were air-dried, scanned and analyzed using the ImageJ plug-in ColonyArea as previously described.[49]

3D-multicellular spheroid assay and spheroid collagen invasion assay:

To inhibit the cells from adhering to the bottom of the cell culture dish, but form 3D-multicellular spheroids instead, 96-well plates had to be precoated by incubating 50 µL per well of 1.5%w/v noble agar (Difco, Cat.No. 5308689) solubilized in base RPMI (Sigma, Cat.No. R0883) for 1h at room-temperature and under ultraviolet iradiation. Per well 4000 cells were seeded and incubated at 37°C until they formed compact spheroids (3-4 days).

The formed spheroids were either treated directly for drug response assessment or embedded into 60 µL of a collagen I-mixture in a novel noble-agar precoated 96-well, to evaluate collagen-invasion capabilities with or without treatment. In any case, the medium (with or without treatment) was exchanged every 72h. The collagen I-mixture consisted of 2.3 mL type I rat tail collagen (Corning, Cat.No. 354236) adjusted to 3.3 mg/mL with 0.02N acetic acid, 570 µL DMEM (Gibco, Cat.No. 11960-044), 25 µL L-Glutamine (Gibco, Cat.No. 25030-024), 30 µL FCS (company, Cat.No.) and 60 µL of 7.5% Sodium-Bicarbonate in PBS. To avoid preliminary polymerization, the collagen-mix was never prepared in larger amounts and always on ice. The spheroids were photographed over a period of 12-14d. The spheroids were photographed over a period of 12-14d. Live/dead fluorescent staining was performed with a staining solution of serum-free RPMI with 8 µM calcein AM (live) (Sigma, Cat.No. 17783) and 10 µM ethidium homodimer (death) (Sigma, Cat.No. 46043). The spheres were assessed by 8 µM calcein AM (live) (Sigma, Cat.No. 17783) and 10 µM ethidium homodimer (death) stain (Sigma, Cat.No. 46043).

Endothelial-cell adhesion assay:

The immortalized microvascular endothelial cells hMEC1 and hCMEC/D3 were seeded into a corning 4-well chamber slide (Falcon, Cat.No. 354114) (25'000 cells per 1.7cm^2 chamber) and grown to 100% confluency (ca 4d). Prior to the adhesion assays the melanoma cell lines were starved with RPMI complete with 1% FCS overnight. On the day of the assay, the cells were detached with trypsin, resuspended in serum-containing medium, washed with PBS and stained with the fluorescent dye Vybrant DiI (1 µg/mL, ThermoFisher, Cat.No. V22885) in serum-free RPMI for 30min at 37°C. The stained cells were then centrifuged, washed, seeded into the chambers (50'000 cells per 1.7cm^2 chamber) in serum-free RPMI and incubated at 37°C for the indicated amount of time. The slides were then washed three times with PBS and fixed with 4% formaldehyde for 20 min at room-temperature. The chambers were then removed and the slides covered with glycerol 50% v/v in PBS and a cover slip. Per well, 5 pictures were taken at 20x, and the fluorescent cells were counted.

Immunostainings

Immunoblot: Cells were detached by trypsin, resuspended in serum-containing cell culture medium, washed with cold PBS and lysed by snap-freezing at -80°C for 30min in cell lysis buffer. The cell lysis buffer contained the following components: NaCl 150mM, MgCl2 15mM, EGTA 1mM, Hepes 50mM, Glycerol 10%, Triton-X 1% solved in ddH2O and the pH adjusted to 7.5. The buffer was supplemented with the phosphatase inhibitor cocktail PhosSTOP EASYpack (1 tablet per 10mL, Roche, Cat.No 05892970001) and protease inhibitor cOmplete ULTRA Tablets (1 tablet per 10mL, Roche, Cat.No 04906845001). The remaining cell debris was centrifuged (4°C, 21'000 rcf, 15min) and the protein-containing supernatant was collected and standardized to equal amounts. We used the following antibodies for immunoblots, some of which were also used for immunohistochemical stains if not stated otherwise: STK11 (CST

#3047), ERK1/2 (CST #4695), p-ERK1/2 T202/Y204 (CST# 4376), STAT3 (CST #9132), p-STAT3 Y705 (#9138), p-STAT3 S727 (CST #9134), FAK (CST #3285), p-FAK Y397 (CST #3283), p-STAT5A/B Y699/Y694 (CST #9359S) For immunohistochemical stainings, the cool IHC machine was used! We used Dako Target Retrieval Solution pH9 for all stainings. The following antibodies were used specifically for IHC: STK11 (SantaCdruz, Cat.No. sc-374334), S100 (Novocastra, Cat.No. NCL-L-S100).

The TMAs with melanoma primary tumors (TMA18 and TMA19) were a gift from the URPP biobank Zurich, University Hospital Zurich, Switzerland (Mitch Levesque). The TMA with melanoma metastases from different origins was purchased from Biomax (Cat.No. BCC38218). The brain metastasis TMA was a gift from Ruth Lyck, University of Bern, Switzerland. TMA analysis was performed with QuPath, closely following the "QuPath TMA CD3 analysis" manual on github (https://github.com/qupath/qupath/wiki/TMA-CD3-analysis).

Human Phospho-Kinase Array Kit

The Proteome Profiler Human Phospho-Kinase Array Kit (R&D systems, Cat. No. ARY003B) was used. 2.5 Mio cells were seeded into a T175 flask and treated with LGX (20nM) or DMSO 48h after seeding for another 24h. Per condition, 5.0 Mio cells were lysed in 0.5mL of the kit lysis buffer. The protein was lysed, and each sample was adjusted to 600ng before following the kit instruction. The exposed blots were analyzed using ImageJ.

Zebrafish husbandry

Zebrafish methods adapted from 2020 Tiso Paper (https://www.osapublishing.org/boe/fulltext.cfm?uri=boe-11-8-4651&id=433823)

Zebrafish xenograft experiments were performed in collaboration with Professor Natascia Tiso at the zebrafish facility of the University of Padova, Italy. Zebrafish strains were maintained according to standard procedures[50]. Fish maintenance and handling was carried out in accordance with European and Italian law on animal experimentation (D.L. 4 March 2014, no. 26), under authorization no. 407/2015-PR from the Italian Ministry of Health.

Zebrafish xenografts

For the injection, the cells were detached with trypsin, resuspended in serum-containing cell culture medium, washed with PBS and stained with the fluorescent dye Vybrant DiI (1 µg/mL, ThermoFisher, Cat.No. V22885) in serum-free RPMI for 30 min at 37°C. The stained cells were then centrifuged, washed with PBS and resuspended in serum-free RPMI at a concentration of 1x10^6 cells per 10 µL. The cells were injected into zebrafish embryos at 2 days post-fertilization (dpf). Immediately before xenografting the cells, the embryos were anesthetized with a solution of tricaine (160 mg/L; Sigma-Aldrich, Cat. No. A5040), embedded in 2% (w/v) methylcellulose (Sigma-Aldrich, Cat.No. A9414) in fish water (150 mg/L Instant Ocean, 6.9 mg/L NaH2PO4, 12.5 mg/L Na2HPO4, pH 7.2) and mounted on a custom-made multi-lane plastic support. The cells were injected into the yolk as a single droplet (100 µm diameter, about 100 cells/embryo), using a WPI microinjector. At 1-day post injection (dpi), the fish were assessed for successful yolk-injection and kept in fish water with either DMSO or the BRAFi LGX818 at 10 nM until 6dpi. The cells were then fixed and assessed for fluorescent-positive metastasis formation under fluorescence microscopy (Leica M165 FC microscope with DFC7000T camera).

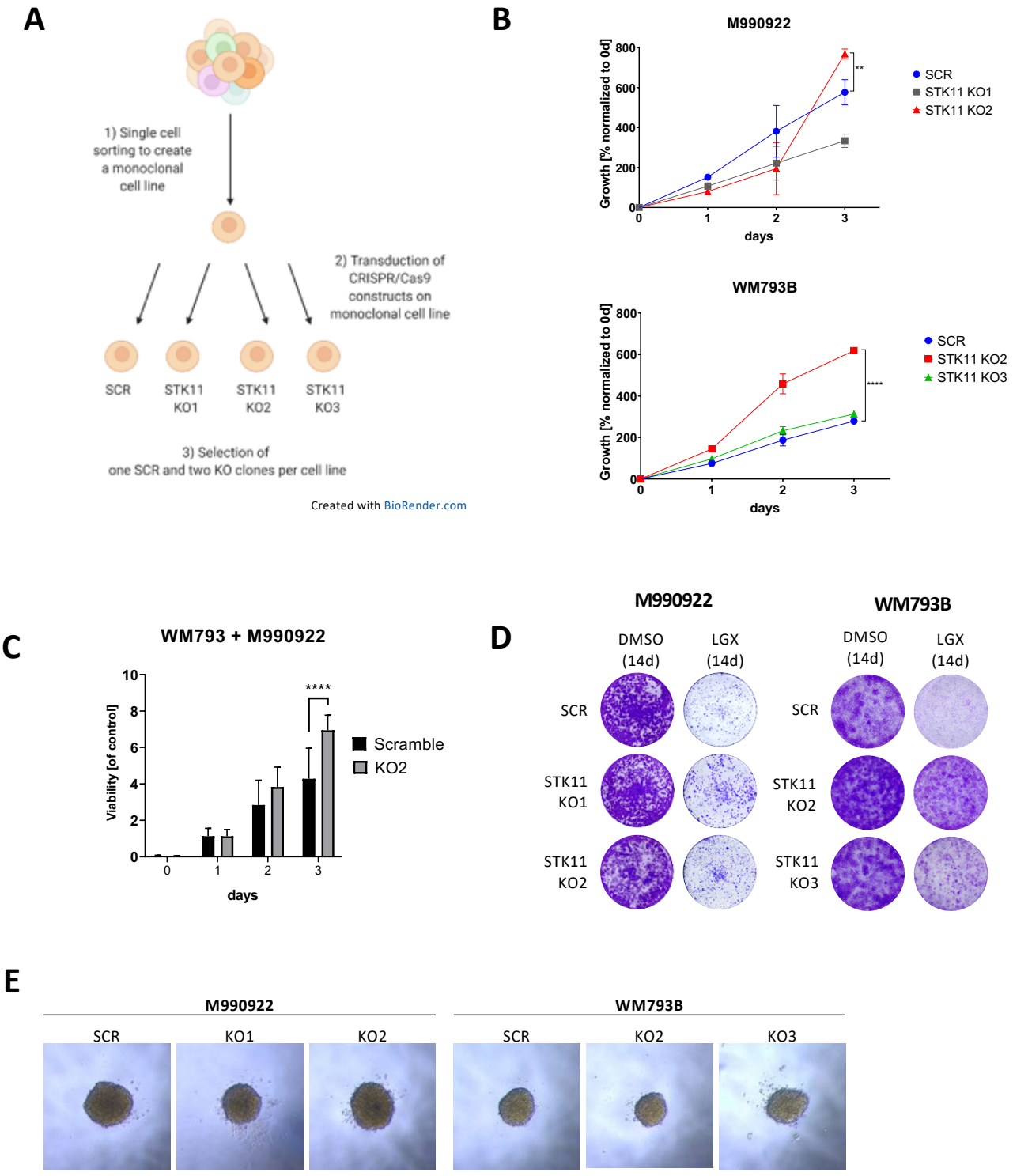

Figure S1 Evaluation of STK11 constructs viability A) Transgenic cell line generation. For both cell cultures, M990922 and WM793B, a monoclonal cell line was created. These cell lines were transduced with SCR (non-targeting sgRNA), STK11 KO1, STK11 KO2 and STK11 KO3 sgRNA/Cas9 constructs. For each cell line, one SCR and two KO-clones were amplified. B) and C) MTT assay of STK11 SCR vs STK11 KO. Data represent the mean ± S.D. of triplicate determinations. Two-way Anova was used for statistical analysis *p<0.05; **p<0.01; ***p<0.001; ****p<0.00001 D) Colony formation assay. 3500 cells per well were seeded into a 24w plate and treated with LGX 10nM. E) 3D multicellular cells successfully formed 4d after seeding 4000 cells per well into an agarose coated 96 well plate.

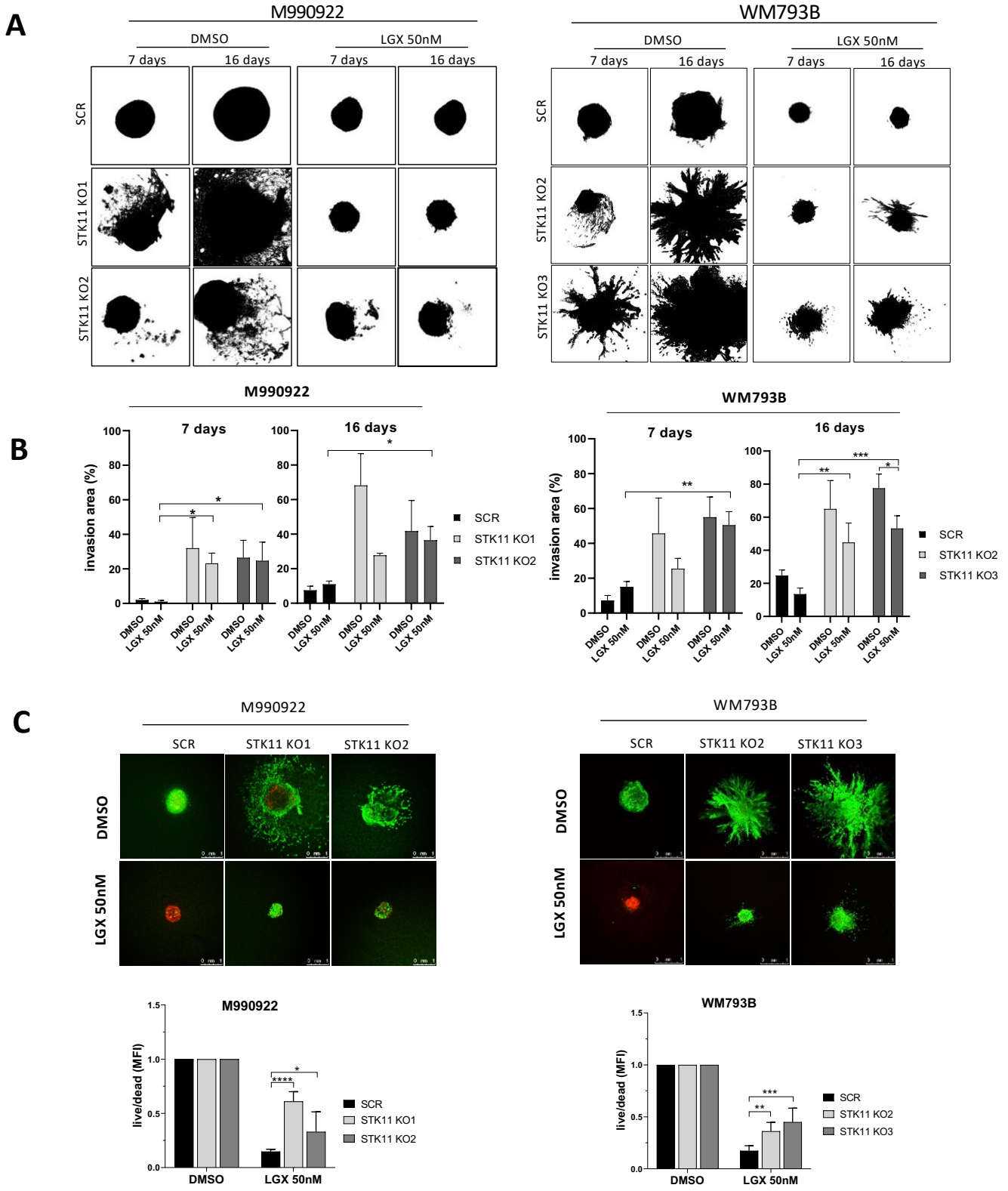

Figure S2 Evaluation of sensitivity to BRAFi in SCR vs STK11 KO melanoma cells in 2D and 3D models

A) Collagen-embedded spheroids were treated with LGX 50nM for 7d and 16d. B) 3 spheres/condition were used to calculate the area of invasion. Two-way Anova was used for statistical analysis. *p<0.05; **p<0.01; ***p<0.001 C) 3D spheres were treated with LGX for 16d and viability was evaluated by Calcein-AM/Ethidium homodimer staining. Live/dead ratio was quantified with Photoshop. 6 spheres/condition were quantified. Two-way Anova was used for statistical analysis. *p<0.05; **p<0.01; ***p<0.001

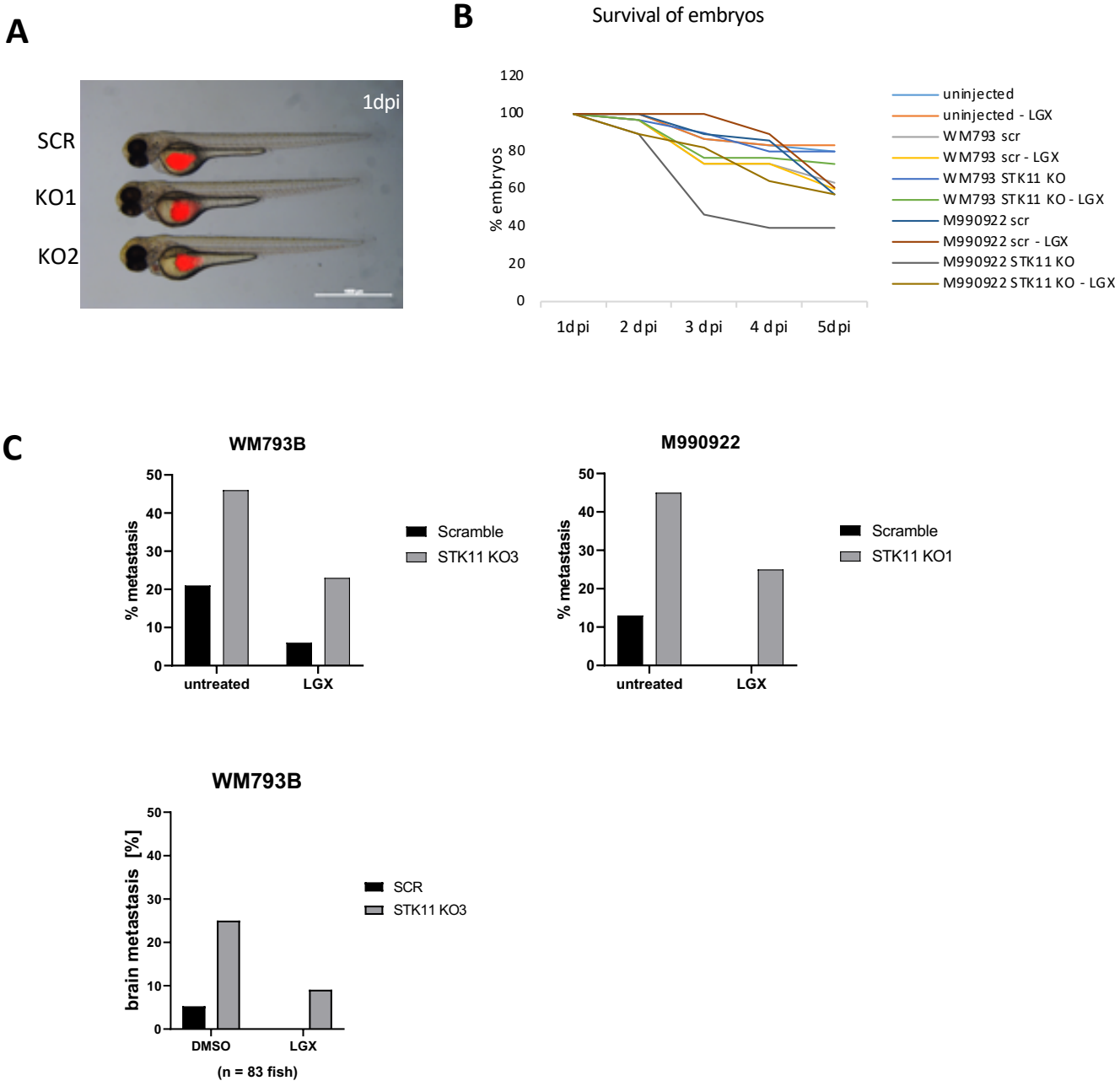

Figure S3 Evaluation of metastasis formation in SCR vs STK11 KO injected zebrafish larvae

A) The yolk of 2d old Zebrafish larvae was injected with human melanoma cell lines and assessed on the next day (1dpi) for successful injection, before treatment start. B) The survival of the embryos under vehicle and LGX treatment, was assessed until 6d. C) and D) At 6d post-transplantation under vehicle and LGX treatment, the injected fish were assessed for fluorescently-labeled metastases outside the yolk for both, M990922 and WM793B by a blind investigator. D) Evaluation of brain metastasis in SCR and STK11 KO injected zebrafish

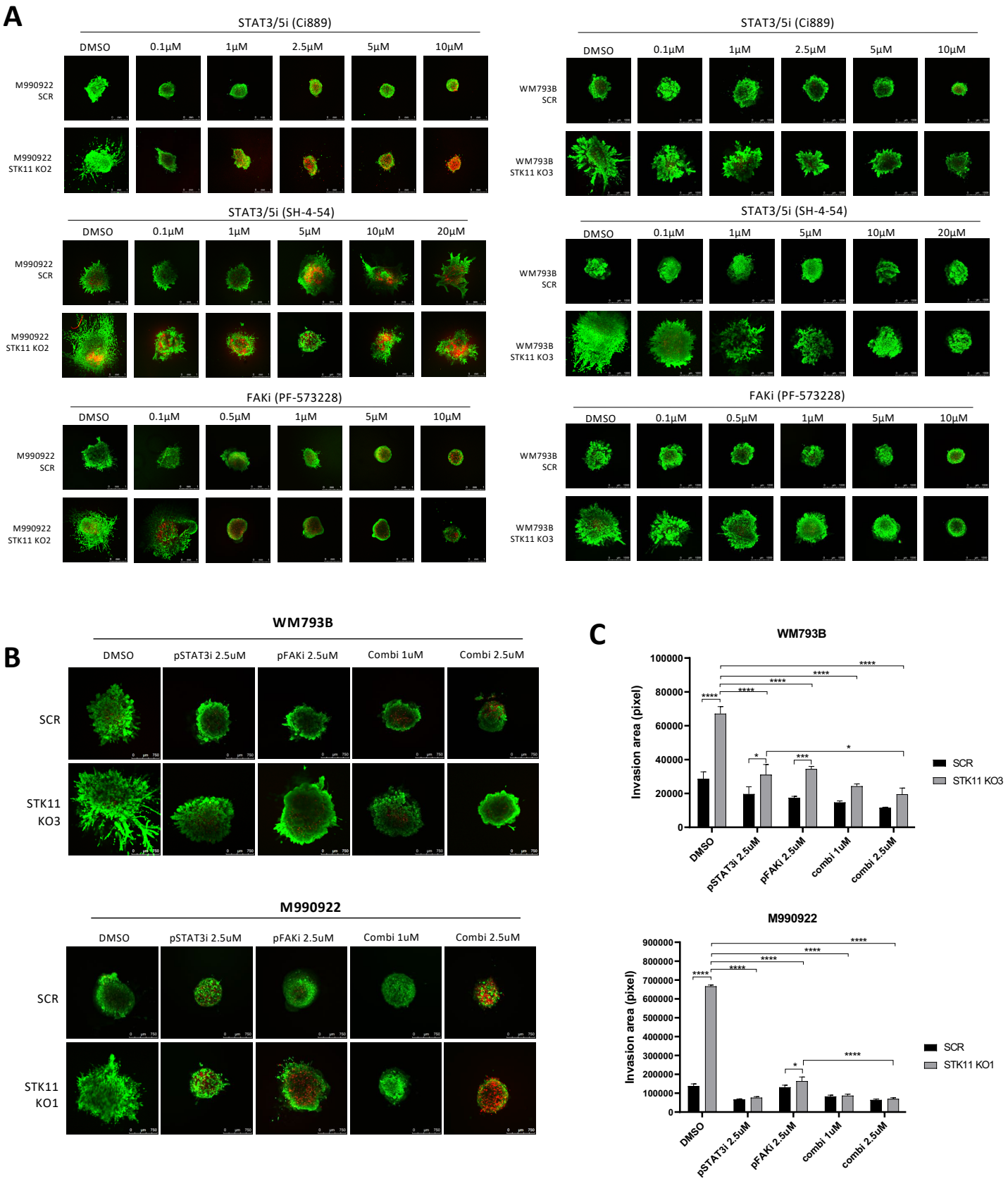

Figure S4 The treatment with pSTAT3/5i and/or pFAKi reverts the invasive phenotype of STK11 KO spheres. A) and B) M990922 and WM793B were treated with increasing concentrations of STAT3/5 (SH-45-4 and C188-9) and FAK (PF-573228) –inhibitors alone or in combination. After 16d the viability of spheres was assessed by Calcein-AM/Ethidium homodimer staining. C) Live/dead ratio was quantified with Photoshop. 6 spheres/condition were quantified. Two-way Anova was used for statistical analysis. *p<0.05; **p<0.01; ***p<0.001